Molecular Pharmacology Fast Forward. Published on July 7, 2022 as DOI: 10.1124/molpharm.122.000549
This article has not been copyedited and formatted. The final version may differ from this version.

TITLE PAGE

TITLE: Optimized pyridazinone nutrient channel inhibitors are potent and specific antimalarial leads

AUTHORS: Michelle M. Butler, Samanthi L. Waidyarachchi, Jinfeng Shao, Son T. Nguyen, Xiaoyuan Ding, Steven C. Cardinale, Lucas R. Morin, Steven M. Kwasny, Mai Ito, Jeanine Gezelle, Maria B. Jiménez-Díaz, Iñigo Angulo Barturen, Robert T. Jacobs, Jeremy N. Burrows, Zachary D. Aron, Terry L. Bowlin and Sanjay A. Desai

Microbiotix, Inc. One Innovation Dr., Worcester, MA, USA (M.M.B., S.L.W., S.T.N., X.D., S.C.C., L.R.M., S.M.K., Z.D.A., T.L.B.)

Laboratory of Malaria and Vector Research, NIAID, National Institutes of Health, Rockville, MD, USA (J.S., M.I., J.G., S.A.D.)

The Art of Discovery, SL, Biscay, Basque Country, Spain (M.B.J.-D., I.A.-B.)

Medicines for Malaria Venture, Geneva, Switzerland (R.T.J., J.N.B.)

Molecular Pharmacology Fast Forward. Published on July 7, 2022 as DOI: 10.1124/molpharm.122.000549
This article has not been copyedited and formatted. The final version may differ from this version.

RUNNING TITLE PAGE

Running title: Pyridazinone antimalarial leads

Corresponding author: Michelle M. Butler, Microbiotix, Inc., 1 Innovation Drive, Worcester, MA 01605; (508) 757-2800; mbutler@microbiotix.com

Numbers of pages, items, words:

Number of text pages: 22

Number of Tables: 0

Number of Figures and Schemes: 5

Number of References: 43

Words in Abstract: 197

Words in Introduction: 462

Words in Discussion: 601

List of non-standard abbreviations:

ADME; absorption, distribution, metabolism, excretion

AUC; area under the curve

BID; twice daily

hEr; human erythrocytes

IV; intravenous

PGIM; physiological growth inhibition medium

PK; pharmacokinetics

PO; oral

PSAC; plasmodial surface anion channel

Molecular Pharmacology Fast Forward. Published on July 7, 2022 as DOI: 10.1124/molpharm.122.000549
This article has not been copyedited and formatted. The final version may differ from this version.

QD; once daily

SAR; structure-activity relationship

Molecular Pharmacology Fast Forward. Published on July 7, 2022 as DOI: 10.1124/molpharm.122.000549
This article has not been copyedited and formatted. The final version may differ from this version.

Abstract

Human and animal malaria parasites increase their host erythrocyte permeability to a broad range of solutes as mediated by parasite-associated ion channels. Molecular and pharmacological studies have implicated an essential role in parasite nutrient acquisition, but inhibitors suitable for development of antimalarial drugs are missing. Here, we generated a potent and specific drug lead using *Plasmodium falciparum*, a virulent human pathogen, and derivatives of MBX-2366, a nanomolar affinity pyridazinone inhibitor from a high-throughput screen. As this screening hit lacks the bioavailability and stability needed for *in vivo* efficacy, we synthesized 315 derivatives to optimize drug-like properties, establish target specificity, and retain potent activity against the parasite-induced permeability. Using a robust, iterative pipeline, we generated MBX-4055, a derivative active against divergent human parasite strains. MBX-4055 has improved oral absorption with acceptable *in vivo* tolerability and pharmacokinetics. It also has no activity against a battery of 35 human channels and receptors and was refractory to acquired resistance during extended *in vitro* selection. Single-molecule and single-cell patch-clamp indicate direct action on the plasmodial surface anion channel, a channel linked to parasite-encoded RhopH proteins. These studies identify pyridazinone as a novel and tractable antimalarial scaffold with a defined mechanism of action.

Molecular Pharmacology Fast Forward. Published on July 7, 2022 as DOI: 10.1124/molpharm.122.000549
This article has not been copyedited and formatted. The final version may differ from this version.

Significance Statement

Because antimalarial drugs are prone to evolving resistance in the virulent human *P. falciparum* pathogen, new therapies are needed. We have now developed a novel drug-like series of pyridazinones that target an unexploited parasite anion channel on the host cell surface, display excellent *in vitro* and *in vivo* ADME properties, are refractory to acquired resistance and demonstrate a well-defined mechanism of action.

Molecular Pharmacology Fast Forward. Published on July 7, 2022 as DOI: 10.1124/molpharm.122.000549
This article has not been copyedited and formatted. The final version may differ from this version.

Introduction

Malaria remains a formidable global health challenge, with *Plasmodium falciparum* and *P. vivax* the main human pathogens that caused an estimated 219 million malaria cases and 409,000 deaths in 2019 (PATH, 2011, WHO, 2020). During the past 20 years, insecticide-impregnated bed nets, vector control, and artemisinin-based combination therapies have reduced morbidity and mortality, but the goals of geographic elimination and global eradication have been thwarted by acquired vector and pathogen resistance (Dondorp et al., 2009, Noedl et al., 2008, Phyo et al., 2012). Chemical screens for small molecules that kill parasites, so-called phenotype screens, have identified many potent antimalarial leads (Gamo et al., 2010, Guiguemde et al., 2010), but are complicated by difficulties of target identification and promiscuous action on multiple parasite activities. The targets of these compounds are typically found through *in vitro* selection of mutants (Luth et al., 2018). While these targets are then considered validated and druggable, their identification through selection of mutants in small-scale experiments also suggests that acquired resistance may arise quickly when the drug is approved for clinical use. Thus, there is a desperate need to develop new therapies with well-defined, but unexploited targets, particularly those refractory to acquired resistance (Anthony et al., 2012, WHO, 2013).

To circumvent the limitations of phenotypic screens, we previously used a cell-based assay to find inhibitors of increased erythrocyte permeability after infection, as has been documented for all examined *Plasmodium* spp. (Kutner et al., 1982, Lisk and Desai, 2005, Wagner et al., 2003). Increased permeability is primarily mediated by the plasmodial surface anion channel (PSAC) linked to the RhopH complex (Counihan et al., 2017, Ito et al., 2017, Mira-Martinez et al., 2013, Nguitragool et al., 2011), but there may also be contributions from upregulated host channels (Bouyer et al., 2020, Dickerman et al., 2016, Staines et al., 2007). Using laboratory strains under *in vitro* conditions, these permeability changes mediate uptake of essential nutrients and

Molecular Pharmacology Fast Forward. Published on July 7, 2022 as DOI: 10.1124/molpharm.122.000549
This article has not been copyedited and formatted. The final version may differ from this version.

dramatically remodel host erythrocyte cation composition (Pillai et al., 2013, Pillai et al., 2012).

A cell-based screen for inhibitors of the parasite-induced permeability identified a potent and tractable pyridazinone scaffold effective against *in vitro* parasite cultures (Pillai et al., 2012). Using hit compound MBX-2366 (ISG-21, Figure 1) as a starting point, we have now engaged in a systematic medicinal chemistry campaign to define the structure-activity relationship for PSAC block and *in vitro* parasite killing. We identified potent derivatives that address the primary liabilities of this scaffold, which included low oral absorption and rapid hepatic metabolism. Single-channel and single-cell electrophysiology studies revealed that our lead compound, MBX-4055 (Figure 1), acts directly on PSAC to quantitatively abolish parasite-induced permeability changes. MBX-4055 has an encouraging preclinical safety profile, is active against geographically divergent, multi-drug resistant *P. falciparum*, and is refractory to acquired resistance under extended *in vitro* selective pressure.

Molecular Pharmacology Fast Forward. Published on July 7, 2022 as DOI: 10.1124/molpharm.122.000549
This article has not been copyedited and formatted. The final version may differ from this version.

Materials and Methods:

Chemical synthesis. All commercially obtained reagents and solvents were used as received. 1H and 13C NMR spectra were recorded on a Bruker 300 MHz instrument. Chemical shifts are given in δ values referenced to the internal standard tetramethylsilane. LC/MS analyses were performed on a Thermo-Finnigan Surveyor LC unit connected to a Thermo LTQ Fleet MS unit. HPLC purification was performed on a Gilson Unipoint instrument equipped with a 00G-4252-P0-AX C18, 10 µm, 150 mm or 250 mm × 21.2 mm column from Phenomonex. Silica gel column purification was performed on Isco brand Combi-flash Rf liquid chromatography system using 50 µm silica Luknova SuperSep columns. Melting points taken on EZ-Melt automated melting point apparatus (Stanford Research Systems, Inc.) in manual mode, and are uncorrected. Thin-layer chromatography was performed on silica gel GHLF plates from Analtech (Newark, DE), and the chromatograms were visualized under UV light at 254 nm. Chlorosulfonic acid and dimethylamine were purchased from Sigma-Aldrich (St. Louis, MO); 4-oxo-4-(thiophen-2-yl)butanoic acid was purchased from Combi blocks (San Diego, CA, USA); Sodium 3-nitrobenzenesulfonate hydrate was purchased from Asta Tech (Bristol, PA,, USA); Phosphorous pentachloride was purchased from Strem Chemicals (Newburyport, MA, USA); piperazine derivatives were purchased from Enamine (Kyiv, Ukraine); N, N-Diisopropylethyl amine, and all solvents were purchased from Millipore-Sigma (St. Louis, MO, USA). As shown in Supplemental Scheme 1, synthesis of the pyridazinones (MBX-4055) were initiated by condensation of readily available 4-oxo-4-(thiophen-2-yl)butanoic acid **1**, and hydrazine hydrate followed by dehydrogenation of compound **2** using sodium 3-nitrobenzenesulfonate to form the corresponding pyridazinone **3** (Fang et al., 2010). Upon treatment of **3** with chlorosulfonic acid, the resulting sulfonyl chloride **4** was then reacted with selected amine **5,** providing the sulfonamide, **MBX-4055** [Scheme 1 (Fang et al., 2010, Sengupta et al., 2015)].

Synthesis of sulfonyl chloride intermediates.

Molecular Pharmacology Fast Forward. Published on July 7, 2022 as DOI: 10.1124/molpharm.122.000549
This article has not been copyedited and formatted. The final version may differ from this version.

Formation of 5-(6-oxo-1,6-dihydropyridazin-3-yl)thiophene-2-sulfonyl chloride (Compound I):

Step 1: To a flask containing 4-oxo-4-(thiophen-2-yl)butanoic acid (110.0g, 597 mmol, 1.0 eq) and hydrazine hydrate (152.5 g, 299 mmol, 5.0 eq) was added EtOH (660 mL). The mixture was heated at 100 °C reflux for 7 h with stirring and the yellowish reaction product precipitated during the reaction. The mixture was cooled and filtered under reduced pressure and rinsed thoroughly with water. The crude product was recrystallized with EtOAc (400 mL) at ice-water bath to give 6-(thiophen-2-yl)-4,5-dihydropyridazin-3(2H)-one as yellow solid (65.2 g, 361 mmol, 61% yield ^{1}H NMR (DMSO-d_6): δ 10.85 (s, NH), 7.61 (d, 1H), 7.44 (d, 1H), 7.10 (m, 1H), 2.97 (t, 2H), 2.46 (t, 2H); MS: 181.0 (M+1).

Step 2: To a flask containing 6-(thiophen-2-yl)-4,5-dihydropyridazin-3(2H)-one (70.0 g, 388 mmol, 1 eq) was added H_2O (8 mL), sodium 3-nitrobenzenesulfonate hydrate (6.12 g, 271mmol, 0.7 eq) and NaOH (38.8 g, 971 mmol, 2.5 eq) at 25 °C. The mixture was heated at 100 °C for 2 h with stirring. The resultant reaction mixture was filtered and adjusted to pH=5-6 with 1 M HCl solution. The residue was purified by column chromatography on silica gel with petroleum ether /ethyl acetate (10:1-1:3) to give 6-(thiophen-2-yl)pyridazin-3(2H)-one (36.5 g, 204 mmol, 53% yield) as light yellow liquid, MS: 179.0 (M+1).

Step 3: PCl_5 (29.2 g, 140mmol, 1 eq) and chlorosulfonic acid (40.9 g, 350mmol, 23.4 mL, 2.5 eq) were added to a 500 mL three-necked round bottom flask equipped with a magnetic stirrer at 0 °C. Then 6-(thiophen-2-yl)pyridazin-3(2H)-one (25.0 g, 140mmol, 1 eq) in $CHCl_3$ (175 mL) was slowly added to the above mixture at 0 °C over 30 min and the mixture was warmed to 25 °C and stirred for 5 h. The reaction mixture was carefully poured into ice water; the resulting yellow solid was collected by filtration, rinsed with water and dried in vacuum to provide crude product. The crude product was recrystallized with MTBE/ petroleum ether (1:1) to give 5-(6-oxo-1,6-dihydropyridazin-3-yl)thiophene-2-sulfonyl chloride (**I**) (13.8 g, 44%, 95% purity) as a

Molecular Pharmacology Fast Forward. Published on July 7, 2022 as DOI: 10.1124/molpharm.122.000549
This article has not been copyedited and formatted. The final version may differ from this version.

light yellow solid ^{1}H NMR (DMSO-d_6): δ 14.51 (brs, NH), 7.99 (d, 1H), 7.45 (d, 1H), 7.07 (d, 1H), 6.93 (d, 1H); MS: 277.2 (M+1).

Formation of 5-(4-methyl-6-oxo-1, 6-dihydropyridazin-3-yl)thiophene-2-sulfonyl chloride (Compound II):

Step 1: A flask containing glyoxylic acid monohydrate (4.17 g, 45.3 mmol) and 1-(thiophen-2-yl)propan-1-one (19.0 g, 135 mmol) in water (20 mL) was heated at 130 °C for 16 h. The mixture was cooled to room temperature and neutralized by adding a mixture of water (20 mL) and NH_4OH (3 mL, 28-30% aqueous solution). The excess remaining 1-(thiophen-2-yl)ethenone was then removed by extraction with CH_2Cl_2 (10 mL x 2). Hydrazine hydrate (2.2 mL) was added to the resulted aqueous layer and the mixture was heated at reflux for 16 hrs. After cooling to room temperature, the liquid was decanted off and methanol (3 mL) was added to the remaining waxy solid. After filtering the resulting suspension, the solid was rinsed with methanol and dried in *vacuo* to yield 5-methyl-6-(thiophen-2-yl)pyridazin-3(2*H*)-one as a yellow solid (2.55 g, 29%); ^{1}H NMR (DMSO-d_6): δ 13.14 (br s, 1H), 7.64 (d, 1H), 7.48 (d, 1H), 7.50 (dd, 1H), 6.83 (s, 1H), 2.37 (s, 3H); MS: 193.0 (M+1).

Step 2: To a flask containing $CHCl_3$ (10 mL), cooled in an ice bath, was slowly added $ClSO_3H$ (1 mL). After 10 min, 5-methyl-6-(thiophen-2-yl)pyridazin-3(2*H*)-one (0.69 g, 3.6 mmol) was added in portions over 30 min. The reaction mixture was allowed to warm to room temperature. After 8 h, the reaction mixture was poured onto ice. The resultant yellow solid was collected by filtration, rinsed with water and dried in *vacuo* to yield 5-(4-methyl-6-oxo-1, 6-dihydropyridazin-3-yl)thiophene-2-sulfonyl chloride as a yellow solid (0.7 g, 67%, >98% purity); ^{1}H NMR (DMSO-d_6): δ 13.09 (br s, NH), 7.26 (d, 1H), 7.09 (d, 1H), 6.83 (s, 1H), 2.36 (s, 3H); MS: 291.1 (M+1).

Method A: General synthesis of sulfonamides

Molecular Pharmacology Fast Forward. Published on July 7, 2022 as DOI: 10.1124/molpharm.122.000549
This article has not been copyedited and formatted. The final version may differ from this version.

N,*N*-diisopropylethylamine (1.5 eq) was added to a flask containing the corresponding sulfonyl chloride (1.0 eq) and piperazine (1.0 eq) in DMF (0.13 M). The reaction was stirred at room temperature under argon atmosphere for 2-12 hrs. Upon completion, the reaction mixture was added to water, and the resulting precipitate was filtered and dried. Impure precipitates were purified with HPLC (5–95% MeCN/H_2O + 0.1% TFA).

Synthesis of 5-((4-(2,5-dimethylphenyl)piperazin-1-yl)sulfonyl)-*N*,*N*-dimethylthiophene-2-carboxamide (MBX-3248):

Step 1*:* Triethylamine (0.120 mL, 1.3 eq) was added to a flask containing methyl 5-(chlorosulfonyl)thiophene-2-carboxylate (150 mg, 0.67 mmol, 1.0 eq) and 1-(2,5-dimethylphenyl)piperazine (153 mg, 0.80 mmol, 1.2 eq) in dichloromethane (4.0 mL); this reaction was stirred at room temperature for 18 h. The mixture was then diluted with water (10 mL) before extracting the aqueous layer with CH_2Cl_2 (2 x 10 mL). The combined organics were dried over anhydrous Na_2SO_4, filtered and concentrated under reduced pressure and dried under vacuum to give desired product quantitatively as a yellow solid. The resultant compound (295 mg, 0.67 mmol, 1.0 equiv.) was dissolved in THF/H_2O (1:1, 0.04 M) and to it was added 21.0 mL of 1 N $LiOH_{(aq)}$ and stirred at room temperature for 18 h. The volatiles were removed and the resultant aqueous layer was acidified to pH~2 using 2 N HCl. The formed precipitate was filtered and washed with hexanes (3x5 mL) and dried in *vacuo* to yield 0.306 g of product, which was used for the next reaction without further purification, MS: 381 (M+1). ^{1}H NMR (DMSO-d_6): δ 7.84 (d, 1H), 7.70 (d, 1H), 7.00 (d, 1H), 6.89 (s, 1H), 6.78 (d, 1H), 3.34 (s, 4H), 2.93 (s, 4H), 2.23 (s, 3H), 2.10 (s, 3H).

Step 2: To a solution of 5-((4-(2,5-dimethylphenyl)piperazin-1-yl)sulfonyl)thiophene-2-carboxylic acid (306 mg, 0.80 mmol, 1.0 eq) in CH_2Cl_2 (0.15 M) was added DMF (0.50 mL, 3.0 eq) followed by cooling in an ice-water bath. Oxalyl chloride (0.3 mL, 2.0 eq) was then added. After warming to room temperature and stirring for 1 hr, the reaction mixture was bubbled with Me_2NH gas for

Molecular Pharmacology Fast Forward. Published on July 7, 2022 as DOI: 10.1124/molpharm.122.000549
This article has not been copyedited and formatted. The final version may differ from this version.

a few minutes and stirred at room temperature from 1-5 h. The reaction was monitored by TLC. After the reaction was complete, water (10 mL) was added and the organics were separated. The aqueous layer was extracted with CH_2Cl_2 (2 x 10 mL). All the organics were combined, dried over anhydrous Na_2SO_4, filtered and concentrated to give crude product, which was purified using a silica gel column with EtOAc/DCM 0-40% gradient). Desired fractions were combined and concentrated under reduced pressure and dried in *vacuo* to yield pure desired product as a white solid (225 mg, 69%). ^{1}H NMR (300 MHz, $CDCl_3$) δ 7.49 (d, 1H), 7.36 (d, 1H), 7.06 (d, 1H), 6.84-6.81 (m, 2H), 3.30-3.20 (m, 4H), 3.20-3.15 (m, 6H), 3.02-2.99 (m, 4H), 2.30 (s, 3H), 2.18 (s, 3H) ; MS 408.0 (M + 1); R_f: 0.50 (3% MeOH/CH_2Cl_2).

MBX-2366: Purchased from CreaGen, Inc. ^{1}H NMR (DMSO-d_6) δ 8.11 (d, 1H), 7.85 (d, 1H), 7.68 (d, 1H), 7.03 (d, 1H), 6.98 (d, 1H), 6.82 (s, 1H), 6.75 (d, 1H), 3.11 (m, 4H), 2.91 (m, 4H), 2.21 (s, 3H), 2.07 (s, 3H)); MS: 431.2 (M + 1); mp: 260-263 °C (decomp.); R_f: 0.75 (86:13:1 $CHCl_3$:MeOH:NH_3).

MBX-3301: Prepared according to Method A using Compound II and (2,5-dimethylphenyl)piperazine . 25.0 mg (48%); white solid; ^{1}H NMR ((DMSO-d_6) δ 13.32 (br s, 1H), 7.68 (m, 2H), 7.02 (d, 1H), 6.91 (s, 1H), 6.84 (s, 1H), 6.78 (d, 1H), 3.13 (m, 4H), 2.94 (m, 4H), 2.43 (s, 3H), 2.30 (s, 3H), 2.10 (s, 3H); MS: 445.1 (M + 1); R_f: 0.62 (86:13:1 $CHCl_3$:MeOH:NH_3) mp: 237-240 °C (decomp).

MBX-5066: Purchased from ChemDiv. white solid; ^{1}H NMR ((DMSO-d_6) δ 13.36 (b s, 1H), 7.94 (d, 1H), 7.36 (d, 1H), 7.02 (m, 2H), 6.78 (m, 2H), 3.27 (br s, 4H), 2.88 (brs, 4H), 2.20 (s, 3H), 2.10 (s, 3H); MS: 415.1(M + 1).

MBX-3105: Prepared according to Method A using Compound I and 1-(pyridin-2-yl)piperazine . 239 mg (54%); light brown solid; ^{1}H NMR ((DMSO-d_6) δ 13.30 (br s, 1H), 8.11-8.08 (m, 2H), 7.82 (d, 1H), 7.68 (d, 1H), 7.53 (m, 1H), 7.03 (d, 1H), 6.83 (d, 1H), 6.66 (dd, 1H),

Molecular Pharmacology Fast Forward. Published on July 7, 2022 as DOI: 10.1124/molpharm.122.000549
This article has not been copyedited and formatted. The final version may differ from this version.

3.63 (m, 4H), 3.06 (m, 4H);MS: 404.0 (M + 1); mp: >300 °C ; R_f: 0.47 (86:13:1 $CHCl_3$:MeOH:NH_3).

MBX-2937: Prepared according to Method A using Compound I and 1-(pyridin-3-yl)piperazine . 60 mg (54%); white solid; ^{1}H NMR ($CDCl_3$:DMSO, 2:1, 1% TFA-d) δ 8.52 (d, 1H), 8.18 (d, 1H), 7.87 (*vr br* d, 1H), 7.82 (d, 1H), 7.70 (*br* dd, 1H), 7.55 (s, 2H), 6.97 (d, 1H), 3.55 (m, 4H), 3.25 (m, 4H); MS: 404.3 (M + 1); mp: 287-289 °C ; R_f: 0.51 (86:13:1,$CHCl_3$:MeOH:NH_3).

MBX-3318: Prepared according to Method A using Compound I and 3-(piperazin-1-yl)pyridine-4-carbonitrile. 30 mg (39%); white solid; ^{1}H NMR (DMSO-d_6) δ 13.30 (s, 1H), 8.55 (s, 1H), 8.35 (dd, 1H), 8.13 (dd, 1H), 7.86 (dd, 1H), 7.74 (dd, 1H), 7.70 (d, 1H), 7.05 (d, 1H), 3.50-3.30 (m, 4H), 3.20-3.00 (m, 4H); MS: 429.1 (M + 1); mp: 296.298 °C.

MBX-3477A: Prepared according to Method A using Compound I and 5-(piperazin-1-yl)pyridin-2-amine . 40 mg (19%); yellow solid; ^{1}H NMR (DMSO-d_6): 13.01 (br s, 1H), 8.12 (d, 1H), 7.88-7.84 (m, 2H), 7.71 (d, 1H), 7.63 (br s, 3H), 7.37 (d, 1H), 5.07 (d, 1H), 6.95 (d, 1H), 3.13 (m, 8H); 13MS: 419.2 (M + 1); mp: 147-149°C ; R_f: 0.59 (86:13:1 $CHCl_3$:MeOH:NH_3).

MBX-3976: Prepared according to Method A using Compound I and 2-(piperazin-1-yl)pyrazine. 20 mg (27%); off white solid; ^{1}H NMR DMSO: 13.28 (s, 1H), 8.31(s, 1H), 8.07 (d, 1H), 7.83 (dd, 2H), 7.68 (d, 2H), 7.02 (dd, 1H), 3.66 (m, 4H), 3.11 (m, 4H); MS: 405.1 (M + 1); mp: >300 °C (decomp).

MBX-4055: Prepared according to Method A using Compound I and 2-methyl-3-(piperazin-1-yl)pyrazine . 49 mg (64%); yellow solid; ^{1}H NMR (DMSO-d_6) δ 13.30 (s, 1H), 8.10 (m, 3H), 7.85 (d, 1H), 7.70 (d, 1H), 7.04 (d, 1H), 3.27 (d, 4H), 3.18 (d, 4H), 2.39 (s, 3H);MS: 419.2 (M + 1); mp: >278 °C.

Molecular Pharmacology Fast Forward. Published on July 7, 2022 as DOI: 10.1124/molpharm.122.000549
This article has not been copyedited and formatted. The final version may differ from this version.

MBX-6513: Prepared according to Method A using Compound I and 2-(piperazin-1-yl)pyridin-1-ium-1-olate . 5 mg (61%); white solid; ^{1}H NMR (DMSO-d_6) δ 13.32 (s, 1H), 8.16 (m, 2H), 7.87 (s, 1H), 7.73 (d, 1H), 7.36 (m, 1H), 7.07 (m, 3H), 3.45 (br s, 4H), 3.14 (br s, 4H);MS: 420.1 (M + 1).

Parasite culture. Laboratory-adapted *P. falciparum* lines were cultivated using O+ human erythrocytes obtained from commercial sources (University of Virginia Blood Bank, Charlottesville, VA) at 5% hematocrit in standard media or PGIM, a modified medium with more physiological levels of critical nutrients (Pillai et al., 2012). PGIM was prepared with reduced concentrations of isoleucine and hypoxanthine (11.4 μM and 3.01 μM, respectively; Sigma-Aldrich, St. Louis, MO). Cultures were maintained at 37 ^{o}C under 5% O_2, 5% CO_2, 90% N_2 and synchronized using sorbitol according to standard methods. The clonal lines used were selected to represent the major malaria-endemic regions globally: Dd2 (derived from Indochina), 7G8 (Brazil), HB3 (Honduras), 3D7 (likely South Africa), Pf803 (Cambodia); these lines also cover the range of antimalarial drug resistance phenotypes.

Transport studies using osmotic lysis measurements. Infected erythrocyte permeability to organic solutes and block by transport inhibitors was quantified using a kinetic assay that tracks light transmittance through a suspension of cells (Pillai et al., 2010). Osmotic lysis resulting from uptake of sorbitol, a sugar alcohol with primary uptake via PSAC and negligible permeability in uninfected erythrocytes, produces increased light transmittance. Synchronous trophozoite-stage cultures were enriched with the Percoll-sorbitol method, washed, and resuspended at 37 ^{o}C in lysis buffer (280 mM sorbitol, 20 mM Na-HEPES, 0.1 mg/ml bovine serum albumin, pH 7.4) to initiate sorbitol uptake and osmotic lysis GE Healthcare, Chicago, IL; Sigma-Aldrich, St. Louis, MO). Inhibitors were added from DMSO stock solutions without preincubation. Transmittance of 700 nm light through the cell suspension was then continuously tracked in a DU640 or DU800 spectrophotometer (Beckman Coulter, Brea, CA). Inhibitor $K_{0.5}$ values were calculated from six-

Molecular Pharmacology Fast Forward. Published on July 7, 2022 as DOI: 10.1124/molpharm.122.000549
This article has not been copyedited and formatted. The final version may differ from this version.

point dose responses using locally-developed scripts that interpolate the time required to reach a fractional lysis threshold, based on a two-compartment model of infected cell osmotic lysis in permeant solutes (Wagner et al., 2003). Iterative medical chemistry screens to define the inhibitor-ion channel structure-activity relationship (SAR) relied on single six-point dose response experiments; compounds selected for advancement were subjected to a minimum of three dose response experiments. Inhibitor affinities and solute permeability coefficients obtained from this method match estimates obtained using patch-clamp (Alkhalil et al., 2004).

Parasite growth inhibition assays. Parasite killing by PSAC inhibitors was quantified using a 72 h SYBR Green I-based fluorescence assay that measures parasite nucleic acid in 96-well microplates (Pillai et al., 2012). Synchronized ring-stage cultures of indicated *P. falciparum* lines were washed and seeded at 1% parasitemia and 2% hematocrit in standard RPMI1640 based medium or PGIM. Cultures were maintained at 37 ^{o}C under 5% O_2, 5% CO_2, 90% N_2 for 72 h without medium changes. At harvest, the culture was lysed in 20 mM Tris, 10 mM EDTA, 0.016% saponin, 1.6% Triton X-100, pH 7.5, with SYBR Green I nucleic acid gel stain at a 5000-fold dilution (Thermo Fisher Scientific, Waltham, MA). The microplate was then incubated at RT for 30-45 min without light exposure before fluorescence measurements (excitation, 485 nm; emission, 528 nm). Inhibitor dose response experiments used triplicate well measurements at each concentration. IC_{50} values were estimated after subtraction of background fluorescence from in-plate controls killed with 20 μM chloroquine in the corresponding medium.

Mammalian cytotoxicity. Inhibitor cytotoxicity was quantified by using human HeLa cells (CLL-2; American Type Culture Collection, Manassas, VA) seeded at 4000 cells/well in 96-well plates. Cultures were incubated with individual inhibitors for 72 h at 37°C in minimal essential medium (Invitrogen, Waltham, MA) supplemented with 10% fetal calf serum (Gibco by Thermo Fisher Scientific, Waltham, MA). Cell viability was quantified by using the vital stain 3-(4,5-dimethylthiazol-2-yl)-5-(3-carboxymethonyphenol)-2-(4-sulfophenyl)-2H-tetrazolium, inner salt

Molecular Pharmacology Fast Forward. Published on July 7, 2022 as DOI: 10.1124/molpharm.122.000549
This article has not been copyedited and formatted. The final version may differ from this version.

(MTT, Promega, Madison, WI), as described (Marshall et al., 1995). Mammalian cell toxicity (CC_{50}) is defined as the concentration of inhibitor which decreases cell viability by 50%.

Solubility. The solubility of compounds was determined by the nephelometric method of Bevan (Bevan and Lloyd, 2000); compounds were serially diluted in DMSO (Sigma-Aldrich, St. Louis, MO) and then added to water or alternate aqueous solutions. Results are reported as the highest concentration that does not cause a sharp increase in the slope of the relative absorption/concentration curve on a Nephelostar nephelometer (BMG Labtech, Cary, NC). Additionally, to confirm the nephelometry results, compounds were stirred with the test vehicle at 20 °C for 4 hours. Additional compound was added if complete dissolution was obtained. The mixture was then filtered, and the filtrate assayed by HPLC (Agilent, 6410 QQQ System, Santa Clara, CA) to quantify the amount of compound in solution.

Murine liver microsome and serum stability. These assays predict the stability of compounds when exposed to the liver and to serum *in vivo*. For microsomal stability measurements, compounds (concentration of 1 μM) were incubated with mouse microsomal proteins (Sekisui XenoTech, LLC, Kansas City, KS) for 30 min in buffer with NADPH (Sigma-Aldrich, St. Louis, MO) as described (Houston, 1994) and the resulting samples analyzed by LC/MS (Thermo Electron, LCQFL-10000, West Palm Beach, FL) to quantitate the remaining parent. The resulting data were reported as half-lives in minutes. For serum stability, compounds at 5 μM were exposed to 55% mouse serum (MP Biomedicals, LLC, Santa Ana, CA), at 37 ºC for 60 minutes and the resulting samples analyzed by LC/MS to quantitate the amount of parent consumed. Data were reported as percent of parent remaining.

Murine serum protein binding. Protein binding for 99% mouse serum was determined following the equilibrium dialysis method (Banker et al., 2003). These assays were performed using a 96-well rapid equilibrium dialysis apparatus (Thermo Fisher Scientific, Waltham, MA)

Molecular Pharmacology Fast Forward. Published on July 7, 2022 as DOI: 10.1124/molpharm.122.000549
This article has not been copyedited and formatted. The final version may differ from this version.

according to the manufacturer's instructions. Propranolol and atenolol were included as high- and low-protein binding control compounds in every test run.

Cytochrome P450 inhibition. Cytochrome P450 inhibition predicts compound interference with enzymes that metabolize drugs *in vivo* and was measured using fluorogenic substrates (Cali et al., 2012, Walsky and Obach, 2004). Test compound (3-50 μM) was added to an assay mix (50 μL) containing 200 mM potassium phosphate pH 7.4, 150 μg/mL mouse liver microsomes, 2.5 mM NADPH (Sigma-Aldrich, St. Louis, MO), and 12 μM Luciferin-IPA luminometric substrate (Promega, Madison, WI) specifically designed to detect only CYP450 3A4 activity. The reactions were incubated for 20 minutes at 37 °C and Luciferin Detection Reagent (50 μL, Promega, Madison, WI) with esterase was added to stop the P450 reaction and initiate the light generating reaction with luciferase. Ketoconazole (Sigma-Aldrich, St. Louis, MO) was used as a positive control inhibitor that inhibits CYP450 3A4 activity by greater than 90% at 100 nM. Quinidine (Sigma-Aldrich, St. Louis, MO) was used as a negative control. After incubation at room temperature for 5 minutes, luminescence was read in an Envision plate reader (Perkin Elmer, Billerica, MA) and percent inhibition was calculated.

Caco-2 permeability. The Caco-2 assay predicts the potential for oral bioavailability. Caco-2 cells were applied to wells of a collagen-coated BioCoat Cell Environment (BD Biosciences, Franklin Lakes, NJ) plate as described (Stewart et al., 1995). The test agent was added to the apical (A) side and the amount of permeation was determined on the basolateral (B) side by LC/MS/MS (Thermo Electron, LCQFL-10000, West Palm Beach, FL) analysis. The amount of material on the A and B sides were used to calculate a P_{app} value.

Safety panel studies. *In vitro* safety studies against a panel of 35 receptors, transporters, ion channels and cytochrome P450 enzymes were performed using established protocols by Eurofins Discovery Services.

Molecular Pharmacology Fast Forward. Published on July 7, 2022 as DOI: 10.1124/molpharm.122.000549
This article has not been copyedited and formatted. The final version may differ from this version.

Compound formulations. MBX-2366: 10% dimethylacetamide (Sigma-Aldrich, St. Louis, MO), 10% PS80 (Croda, Princeton, NJ), 80% PEG-400 (Fluka, Sigma-Aldrich, St. Louis, MO); MBX-3318: 10% DMSO, 1% Polysorbate 80, 80% PEG-400; MBX-3477A 5% DMSO, 5% Polysorbate 80, 25% (2-Hydroxpropyl)-β-cyclodextrin (Sigma-Aldrich, St. Louis, MO); MBX-4055: 6.25% DMSO, 12.5% polysorbate 80, 43.75% Labrasol® (Gattefossé, Lyon, France), 1.25% hydroxypropyl methylcellulose (Sigma-Aldrich, St. louis, MO) in H_2O.

Murine pharmacokinetics (PK). Compounds were formulated as described above and male CD-1 mice (n=3) were dosed with single dose levels of test compounds (3 mg/mL, 3.3-10 mL/kg, 10-30 mg/kg) by the intravenous (IV) and oral (PO) routes. Serial blood samples (approximately 20 µL each) were collected at 7 time points per route via tail vein, facial bleed or cardiac puncture following inhalation anesthesia (for terminal bleeds). Samples were processed and compound content analyzed by LC/MS (Thermo Electron, LCQFL-10000, West Palm Beach, FL). PK parameters were calculated using WinNonLin Phoenix 8 (Certara, Princeton, NJ).

Murine tolerability. Compounds were dissolved at concentrations up to 20 mg/mL in various formulations. Male CD-1 mice were dosed with 4 dose levels (vehicle control plus 3 dose levels) of test compound by the IV or PO route. All mice were monitored at dosing and at 1-, 3-, 8-, 24-, 48- and 72-hours post-dose for any adverse effects and all abnormalities (such as lethargy, ataxia, breathing and digestive issues, etc.) were recorded and reported to the study director. Any animals observed to be moribund were euthanized by cardiac puncture with terminal blood collection following inhalation anesthesia.

***In vitro* selection with PSAC inhibitors.** The *P. falciparum* Dd2 clone was used for *in vitro* selections to examine the potential for acquired resistance to MBX-4055. Cultures were seeded at 1-2% starting parasitemia and challenged with MBX-4055 at 600 nM (20x the growth inhibition IC_{50}) in PGIM medium to limit nutrient availability. Cultures were observed by Giemsa

Molecular Pharmacology Fast Forward. Published on July 7, 2022 as DOI: 10.1124/molpharm.122.000549
This article has not been copyedited and formatted. The final version may differ from this version.

staining of thin blood smears with medium replacement every 1-2 days. Drug pressure was maintained until consecutive smears were negative for viable parasites. The culture was then transferred to standard RPMI-based medium (Thermo Fisher Scientific, Waltham, MA) without drugs to allow outgrowth of potential mutants. When the parasites recovered to > 1% parasitemia, an aliquot was taken for cryopreservation before repeating identical cycles of drug challenge and recovery for 6 months. The resulting parasite culture, termed $Dd2_{4055}$, was used for transport and growth inhibition studies.

Electrophysiology. Low-noise patch-clamp recordings were obtained from trophozoite-stage infected cells using the Dd2 strain. Seals were formed with freshly-pulled quartz capillaries with pipette resistances of 2-3 MΩ in symmetrical bath and pipette solutions of 1000 mM choline chloride, 115 mM NaCl, 10 mM MgCl2, 5 mM $CaCl_2$, 20 mM Na-HEPES, pH 7.4 as described previously (Nguitragool et al., 2011). Seal resistances were typically > 100 GΩ. Membrane potentials were applied from a holding potential of 0 mV using an Axopatch 200B amplifier and Digidata 1550 digitizer (Molecular Devices, San Jose, CA). Whole-cell patch-clamp recordings were obtained after application of brief, high-voltage electrical pulses to disrupt the membrane patch. Where indicated, inhibitor was added manually from pre-prepared stock solutions in the above bath solution. Inhibitor dose response experiments were tabulated after subtraction of small leak currents. All recordings were digitized at 100 kHz, filtered at 5 kHz (8-pole Bessel, Frequency Devices), and analyzed with Clampfit 10.0 (Molecular Devices, San Jose, CA) and SigmaPlot 10.0 (Systat, Chicago, IL).

Molecular Pharmacology Fast Forward. Published on July 7, 2022 as DOI: 10.1124/molpharm.122.000549
This article has not been copyedited and formatted. The final version may differ from this version.

Results

Iterative medicinal chemistry yields a potent inhibitor suitable for *in vivo* preclinical studies. On the basis of the inhibition of infected cell permeability by the hit compound MBX-2366, targeted pyridazinones were synthesized in a convergent four–step sequence from readily available starting materials and literature protocols [Figure 1 and Supplemental Scheme 1, (Fang et al., 2010, Sengupta et al., 2015)]. We synthesized a total of 315 pyridazinones, modifying each zone of the molecule (Figure 2A), and used a quantitative but straightforward cell-based permeability assay to drive iterative examination of structure-activity relationship (SAR). Although MBX-2366 displays low nanomolar potency, assessment of its *in vitro* pharmacokinetic properties revealed that the overall ADME profile renders it unsuitable for pre-clinical development (Figure 2B, Figure 1, entry 1). To enable murine efficacy in the humanized mouse model, newly synthesized derivatives were assessed for *in vitro* target potency ($K_{0.5}$) in a transmittance-based erythrocyte osmotic lysis assay [Figure 2C, (Wagner et al., 2003)], growth inhibition activity (IC_{50}) [Figure 2D, (Lisk et al., 2008)], and ADME properties (Figure 1). Improved *in vitro* growth inhibition in assays using PGIM, a medium with more physiological concentrations of key essential nutrients, independently confirmed action against parasite nutrient uptake (red symbols, Figure 2D). These SAR studies demonstrated a high responsiveness to structural changes, consistent with binding specificity between the scaffold and the molecular target. Although target block in *Plasmodium spp.* is often not directly related to parasite killing, we found a statistically significant correlation between PSAC-blocking potency and *in vitro* parasite growth inhibition (Figure 2E, Pearson's correlation coefficient, $r = 0.81$, $P < 10^{-4}$), suggesting that pyridazinones act specifically at the host membrane to inhibit uptake. The pyridazinone scaffold of MBX-2366 is composed of four partially modular units (denoted as "Zones", Figure 2A, Figure 1). Our studies revealed that the pyridazinone moiety (Zone 1) plays a crucial role towards potency, with some replacements reducing the growth inhibition potential

Molecular Pharmacology Fast Forward. Published on July 7, 2022 as DOI: 10.1124/molpharm.122.000549
This article has not been copyedited and formatted. The final version may differ from this version.

of the molecule (Figure 1, entry 2) and substituents on the pyridazinone moiety maintaining potency without impact on overall ADME properties except solubility (entry 3). Similarly, the thiophene ring (Zone 2) plays a critical role in potency and cytotoxicity (entry 4), with very few modifications tolerated. We also observed that variations of the right terminal aromatic group (Zone 4) allow for broad tuning of both potency and ADME properties. For example, changing the xylene of MBX-2366 to a pyridine or substituted pyridine (entries 5-7) improves cytotoxicity and Caco-2 permeability while addition of an amino group (entry 8) improves solubility and stability, albeit to the detriment of membrane permeability. Modification of Zone 4 to a substituted pyrazine improves cytotoxicity, permeability and stability with a moderate improvement in solubility (entry 10) compared to entry 1 and the unsubstituted pyrazine (entry 9).

SAR studies of MBX-2366 identified four candidate leads, MBX-3318, MBX-3477A, MBX-3976 and MBX-4055 (Figure 2B, Figure 1), with favorable ADME properties predicting efficacy in animal studies. Each of these derivatives exhibits excellent potency against solute uptake in infected cells, *in vitro* parasite killing, murine serum stability, and plasma protein binding. Except for MBX-3477A, each also has acceptable membrane permeability in Caco-2 assays, an indicator of oral bioavailability that justifies oral dosing in animal studies. Despite improved murine liver microsomal stability of the lead MBX-4055 over the parent MBX-2366, we identified a metabolic liability within the Zone 4 nitrogen heterocycle, presumably through *N*-oxidation. Accordingly, introduction of a pyridine *N*-oxide in Zone 4 of the scaffold (Figure 1, entry 11), improved the metabolic stability but at the expense of a >10-fold reduction in target potency. *In vitro* analyses also suggested that MBX-4055 may have low toxicity in mammals. Assays for competitive binding with 45 mammalian receptors, inhibition of 7 cardiac ion channels and the 5 major liver CYP450 enzymes (Supplemental Table 1), and an Ames assay for genotoxicity revealed only minor inhibition of one mammalian receptor, indicating a desirable profile with

Molecular Pharmacology Fast Forward. Published on July 7, 2022 as DOI: 10.1124/molpharm.122.000549
This article has not been copyedited and formatted. The final version may differ from this version.

negligible off-target activity, and no genotoxicity (data not shown). Finally, determination of human liver microsome stability for MBX-4055 demonstrated very little difference between human and mouse metabolic stability (half-lives of 24.2 and 26.5, respectively), suggesting that mouse metabolism would be predictive of human metabolism.

Proof-of-concept murine tolerability and pharmacokinetics. Based on preserved *in vitro* potency with improved ADME results of selected derivatives, we advanced compounds MBX-3318, MBX-3477A, MBX-3976 and MBX-4055 to murine studies. As shown in Figures 3A, 3B and Supplemental Table 2, the hit compound, MBX-2366, demonstrated low oral exposure that was improved upon with MBX-3318. MBX-3318 demonstrated improved oral exposure after a single dose in mice (Supplemental Figure 1A, Supplemental Table 2) as well as moderate oral bioavailability. However, poor observed *in vitro* stability resulted in low IV plasma exposure (area under the curve; AUC), a short half-life ($t_{1/2}$), a greater volume of distribution (Vss) and a high clearance rate, making it less than optimal for future efficacy studies. MBX-3477A demonstrated improved IV exposure and half-life (Supplemental Figure 1B, Supplemental Table 2) over that for MBX-3318, but demonstrated poor oral bioavailability as anticipated by a low Caco-2 permeability (Supplemental Table 1). MBX-3976 exhibited excellent IV exposure, moderate oral bioavailability, lower clearance rate and volume of distribution (Supplemental Figure 1C, Supplemental Table 2); however, it had a short oral half-life. In comparison, MBX-4055 revealed greater exposure over 24 hours after a single oral dose (Figure 3A, B), with nearly 3-fold improved oral bioavailability and preserved/improved liver microsome stability (Figure 1), 20-fold greater exposure, a 2-fold longer half-life and 6-fold slower clearance than MBX-3318. Additionally, we administered compounds MBX, 2366, MBX-3318, MBX-3477A, MBX-3976 and MBX-4055 by the IV or PO routes to mice to determine tolerability. As shown in Supplemental Table 3, mice dosed with MBX-2366 by the IV route died immediately; however, dosing by the IV routes of the remaining compounds caused either no adverse effects (MBX-3318, MBX-

Molecular Pharmacology Fast Forward. Published on July 7, 2022 as DOI: 10.1124/molpharm.122.000549
This article has not been copyedited and formatted. The final version may differ from this version.

3477A) or moderate effects that did not require euthanization (MBX-3976, MBX-4055). When dosed by the PO route, only MBX-3318 caused moderate effects of decreased activity, irregular breathing and rough hair coat for up to 8 hours post-dose; the remaining compounds produced only mild, short-lived effects. The maximum tolerated doses for MBX-3976 and MBX-4055 were estimated to be >65 and >100 mg/kg, respectively.

Direct action on PSAC. We examined mechanism of action for the MBX-4055 antimalarial lead and began by determining that this compound exhibits dose-dependent inhibition of uptake of sorbitol (Figure 4A), a sugar alcohol that enters infected cells primarily via PSAC (Pillai et al., 2010). This permeability is conserved amongst divergent *P. falciparum* clones, including those resistant to various antimalarials. MBX-4055 potently blocked uptake in each clone but exhibited modest variation in potency against the target and against *in vitro* parasite growth (Figure 4B, $K_{0.5}$ and IC_{50}, red and black bars, respectively).

To further examine mechanism of action and the potential for acquired resistance, we used *in vitro* selection through cyclical application of 600 nM MBX-4055 (~ 20x IC_{50}) in PGIM until cultures were microscopically sterilized. Between cycles, surviving parasites were allowed to recover in nutrient-rich standard RPMI-based media, permitting stringent selection of resistant mutants. After extensive cycling of high-dose MBX-4055 treatment, the resulting $Dd2_{4055}$ parasite line exhibited unchanged susceptibility to killing by MBX-4055 (Figure 4C). Transport inhibition dose response studies also revealed unchanged MBX-4055 potency against the channel targets in the $Dd2_{4055}$ line (Figure 4D). Finally, overexpression of the PSAC target was excluded by an unchanged sorbitol permeability (Figure 4E). While downregulation of channel-mediated transport after selection with toxins that require PSAC-mediated uptake has been observed (Mira-Martinez et al., 2013, Sharma et al., 2015, Sharma et al., 2013), overexpression of this target risks premature osmotic lysis of infected cells (Cohn et al., 2003). These findings

Molecular Pharmacology Fast Forward. Published on July 7, 2022 as DOI: 10.1124/molpharm.122.000549
This article has not been copyedited and formatted. The final version may differ from this version.

suggest a constrained inhibitor-binding pocket on the channel that is refractory to resistance mutations.

Cell-attached and whole-cell patch-clamp confirmed and extended these findings. We first used conventional cell-attached patch-clamp with MBX-4055 added symmetrically to bath and pipette compartments to ensure channels are exposed to the compound (Figure 5A). In single channel recordings with this configuration, long blocked events (> 1 s) were observed, as previously reported for unrelated potent inhibitors that do not meet our drug-likeness criteria (Nguitragool et al., 2011, Pillai et al., 2010).

We then used a modified cell-attached configuration to circumvent concerns of molecule-to-molecule variation in channel gating (Figure 5B, graphic). Here, a seal was formed on an infected cell without inhibitor; after obtaining baseline channel activity measurements, MBX-4055 was added to the bath compartment. For detectable inhibition under these conditions, the inhibitor must cross into the infected cell and diffuse to its binding site on the channel(s) in the patch; if the binding site is on the extracellular channel face, a second membrane crossing into the pipette is also required. Figure 5B shows a recording from a patch with 3 identical channel molecules. MBX-4055 addition to the bath, at 10x its $K_{0.5}$ value from sorbitol uptake studies, produced block almost immediately after addition (bottom trace). The complex transitions associated with activity from three independent channels was reduced to a primarily closed state with infrequent bursts of openings (Figure 5C). Notably, this configuration provides independent evidence for MBX-4055 membrane permeability, as determined above using Caco-2 permeability studies (Supplementary Table 1).

To obtain more quantitative estimates of PSAC block by MBX-4055, we next used the whole-cell configuration and performed dose response experiments on single cells (Figure 5D). After obtaining inhibitor-free recordings at a range of membrane potentials, MBX-4055 was added in increasing doses with measurements of whole-cell currents after each addition. These

Molecular Pharmacology Fast Forward. Published on July 7, 2022 as DOI: 10.1124/molpharm.122.000549
This article has not been copyedited and formatted. The final version may differ from this version.

dose response experiments revealed quantitative and complete inhibition of whole-cell currents, consistent with PSAC being the primary conductive pathway on the infected erythrocyte membrane (Nguitragool et al., 2011). By combining the dose response measurements from four infected cells, we estimated a $K_{0.5}$ of 136 ± 16 nM for inhibition (Figure 5E), a value somewhat greater than observed in our sorbitol permeability measurements. As these patch-clamp experiments were performed with molar [Cl^-] at both channel faces and the sorbitol uptake studies used isotonic solutions, the higher $K_{0.5}$ values with patch-clamp may reflect competition between permeating solutes and the inhibitor. Because PSAC exhibits low affinity binding for permeating solutes (26), competition between solutes and inhibitors has not been observed in previous studies of this channel. These findings are, nevertheless, consistent with PSAC inhibition as the primary mechanism of action against *P. falciparum*.

Molecular Pharmacology Fast Forward. Published on July 7, 2022 as DOI: 10.1124/molpharm.122.000549
This article has not been copyedited and formatted. The final version may differ from this version.

Discussion

Our studies define pyridazinones as a drug scaffold with a well-characterized mechanism of action distinct from those of existing antimalarial chemotherapies. PSAC and the pyridazinone derivatives have several properties that are ideal for development as part of a combination therapy regimen for malaria cure. First, because PSAC is on the host erythrocyte membrane, it is more accessible to small molecule inhibitors in plasma. In contrast, all currently approved antimalarial drugs must cross at least three membranes to reach their intracellular parasite targets. Antimalarial drugs including chloroquine, mefloquine and possibly artemisinin derivatives are also plagued by acquired resistance via extrusion by organic solute pumps (Krogstad et al., 1987, Veiga et al., 2016). Because such pumps are not present at the host membrane, PSAC inhibitors are not prone to this resistance mechanism. Second, the PSAC target is highly conserved in all examined *Plasmodium* spp. with conductance, gating, selectivity, and pharmacology largely unchanged between *P. falciparum* and the divergent *P. knowlesi* functional ortholog (Lisk and Desai, 2005). We submit that conservation not only of the responsible CLAG, RhopH2, and RhopH3 subunits but also of biophysical properties of channel-mediated permeation have resulted from marked constraints on the channel. Mutations that compromise subunit assembly into the RhopH complex (Counihan et al., 2017, Ito et al., 2017, Schureck et al., 2021), export and host membrane insertion (Ito et al., 2017, Mira-Martinez et al., 2013, Nguitragool et al., 2011), permeability of a broad range of essential nutrients (Bokhari et al., 2008, Kutner et al., 1982), or PSAC's stringently low Na^+ permeability (Cohn et al., 2003, Overman, 1948) would all compromise PSAC's essential role and confer an unacceptable fitness cost. These constraints suggest that acquired resistance in the clinical setting may be limited or arise only after extended use. Third, the availability of robust, quantitative assays for PSAC has enabled the full spectrum of biochemical study, ranging from single-molecule studies of inhibitor action on the channel (Alkhalil et al., 2004), iterative

Molecular Pharmacology Fast Forward. Published on July 7, 2022 as DOI: 10.1124/molpharm.122.000549
This article has not been copyedited and formatted. The final version may differ from this version.

medicinal chemistry with rapid inhibitor-target dose responses with a simple transmittance readout (the present study), and high-throughput screening technologies that have yielded potent and specific lead compounds (Pillai et al., 2010).

Pyridazinones have a distinct mechanism from those of existing antimalarial drugs, as evidenced by dramatically improved parasite killing in PGIM, a nutrient-limited medium that more closely approximate physiological conditions (Pillai et al., 2012). A key limitation of compounds identified in phenotypic screens that have relied exclusively on *in vitro* growth inhibition using nutrient-rich RPMI-based media is that those assays may not reflect parasite growth and killing kinetics in human infections (Gamo et al., 2010, Guiguemde et al., 2010). Although nutrient deprivation is an experimentally validated outcome of PSAC block, the broad range of ions and organic solutes that permeate through this channel suggest that MBX-4055 and other potent PSAC inhibitors may also produce trapping of parasite metabolic waste within infected cells, which is also expected to be lethal to the intracellular parasite (Staines et al., 2007). PSAC's permeability to inorganic cations may also produce changes in erythrocyte rigidity, leading to eryptosis and phagocytosis in the circulation, as has been observed for compounds that interfere with Na^+ transport between host and parasite compartments (Jimenez-Diaz et al., 2014). These potential consequences of PSAC inhibition require more rigorous study. The potent and specific scaffold identified here provides a clear pharmacological avenue for these studies.

Lead compound MBX-4055 is highly specific for the PSAC target without activity against a battery of human channels, enzymes and receptors. Further iterative medicinal chemistry and target studies, enabled by facile and robust assays for PSAC block, are ongoing and may provide curative treatment of malaria.

Molecular Pharmacology Fast Forward. Published on July 7, 2022 as DOI: 10.1124/molpharm.122.000549
This article has not been copyedited and formatted. The final version may differ from this version.

Acknowledgements

We thank Ryan Kissinger and Anita Mora for help with artwork.

Molecular Pharmacology Fast Forward. Published on July 7, 2022 as DOI: 10.1124/molpharm.122.000549
This article has not been copyedited and formatted. The final version may differ from this version.

Authorship Contributions

Participated in research design: Butler, Waidyarachchi, Nguyen, Jiménez-Díaz, Angulo Barturen, Jacobs, Burrows, Aron, Bowlin and Desai.

Conducted experiments: Waidyarachchi, Shao, Nguyen, Ding, Cardinale, Morin, Kwasny, Ito, Gezelle.

Performed data analysis: Butler, Waidyarachchi, Shao, Nguyen, Cardinale, Morin, Kwasny, Ito, Gezelle and Desai.

Wrote or contributed to the writing of the manuscript: Butler, Waidyarachchi, Desai.

Molecular Pharmacology Fast Forward. Published on July 7, 2022 as DOI: 10.1124/molpharm.122.000549
This article has not been copyedited and formatted. The final version may differ from this version.

References

ALKHALIL, A., COHN, J. V., WAGNER, M. A., CABRERA, J. S., RAJAPANDI, T. & DESAI, S. A. 2004. Plasmodium falciparum likely encodes the principal anion channel on infected human erythrocytes. *Blood,* 104**,** 4279-86.

ANTHONY, M. P., BURROWS, J. N., DUPARC, S., MOEHRLE, J. J. & WELLS, T. N. 2012. The global pipeline of new medicines for the control and elimination of malaria. *Malar J,* 11**,** 316.

BANKER, M. J., CLARK, T. H. & WILLIAMS, J. A. 2003. Development and validation of a 96-well equilibrium dialysis apparatus for measuring plasma protein binding. *J Pharm Sci,* 92**,** 967-74.

BEVAN, C. D. & LLOYD, R. S. 2000. A high-throughput screening method for the determination of aqueous drug solubility using laser nephelometry in microtiter plates. *Anal Chem,* 72**,** 1781-7.

BOKHARI, A. A., SOLOMON, T. & DESAI, S. A. 2008. Two distinct mechanisms of transport through the plasmodial surface anion channel. *J Membr Biol,* 226**,** 27-34.

BOUYER, G., BARBIERI, D., DUPUY, F., MARTEAU, A., SISSOKO, A., N'DRI, M. E., NEVEU, G., BEDAULT, L., KHODABUX, N., ROMAN, D., HOUZE, S., SICILIANO, G., ALANO, P., MARTINS, R. M., LOPEZ-RUBIO, J. J., CLAIN, J., DUVAL, R., EGEE, S. & LAVAZEC, C. 2020. Plasmodium falciparum sexual parasites regulate infected erythrocyte permeability. *Commun Biol,* 3**,** 726.

CALI, J. J., MA, D., WOOD, M. G., MEISENHEIMER, P. L. & KLAUBERT, D. H. 2012. Bioluminescent assays for ADME evaluation: dialing in CYP selectivity with luminogenic substrates. *Expert Opin Drug Metab Toxicol,* 8**,** 1115-30.

COHN, J. V., ALKHALIL, A., WAGNER, M. A., RAJAPANDI, T. & DESAI, S. A. 2003. Extracellular lysines on the plasmodial surface anion channel involved in Na+ exclusion. *Mol Biochem Parasitol,* 132**,** 27-34.

COUNIHAN, N. A., CHISHOLM, S. A., BULLEN, H. E., SRIVASTAVA, A., SANDERS, P. R., JONSDOTTIR, T. K., WEISS, G. E., GHOSH, S., CRABB, B. S., CREEK, D. J., GILSON, P. R. & DE KONING-WARD, T. F. 2017. Plasmodium falciparum parasites deploy RhopH2 into the host erythrocyte to obtain nutrients, grow and replicate. *Elife,* 6.

DICKERMAN, B. K., ELSWORTH, B., COBBOLD, S. A., NIE, C. Q., MCCONVILLE, M. J., CRABB, B. S. & GILSON, P. R. 2016. Identification of inhibitors that dually target the new permeability pathway and dihydroorotate dehydrogenase in the blood stage of Plasmodium falciparum. *Sci Rep,* 6**,** 37502.

DONDORP, A. M., NOSTEN, F., YI, P., DAS, D., PHYO, A. P., TARNING, J., LWIN, K. M., ARIEY, F., HANPITHAKPONG, W., LEE, S. J., RINGWALD, P., SILAMUT, K., IMWONG, M., CHOTIVANICH, K., LIM, P., HERDMAN, T., AN, S. S., YEUNG, S., SINGHASIVANON, P., DAY, N. P., LINDEGARDH, N., SOCHEAT, D. & WHITE, N. J. 2009. Artemisinin resistance in Plasmodium falciparum malaria. *N Engl J Med,* 361**,** 455-67.

FANG, Y., LI, Y., WANG, S., MENG, Y., PENG, J. & WANG, B. 2010. Synthesis, characterization and electroluminescence properties of iridium complexes based on pyridazine and phthalazine derivatives with C^N N structure. *Synthetic metals,* 160**,** 2231-38.

GAMO, F. J., SANZ, L. M., VIDAL, J., DE COZAR, C., ALVAREZ, E., LAVANDERA, J. L., VANDERWALL, D. E., GREEN, D. V., KUMAR, V., HASAN, S., BROWN, J. R., PEISHOFF, C. E., CARDON, L. R. & GARCIA-BUSTOS, J. F. 2010. Thousands of chemical starting points for antimalarial lead identification. *Nature,* 465**,** 305-10.

GUIGUEMDE, W. A., SHELAT, A. A., BOUCK, D., DUFFY, S., CROWTHER, G. J., DAVIS, P. H., SMITHSON, D. C., CONNELLY, M., CLARK, J., ZHU, F., JIMENEZ-DIAZ, M. B., MARTINEZ, M. S., WILSON, E. B., TRIPATHI, A. K., GUT, J., SHARLOW, E. R., BATHURST, I., EL MAZOUNI, F., FOWBLE, J. W., FORQUER, I., MCGINLEY, P. L., CASTRO, S., ANGULO-BARTUREN, I., FERRER, S., ROSENTHAL, P. J., DERISI, J. L., SULLIVAN, D. J., LAZO, J. S., ROOS, D. S., RISCOE, M. K., PHILLIPS, M. A., RATHOD, P. K., VAN VOORHIS, W. C., AVERY, V. M. & GUY, R. K. 2010. Chemical genetics of Plasmodium falciparum. *Nature,* 465**,** 311-5.

HOUSTON, J. B. 1994. Utility of in vitro drug metabolism data in predicting in vivo metabolic clearance. *Biochem Pharmacol,* 47**,** 1469-79.

ITO, D., SCHURECK, M. A. & DESAI, S. A. 2017. An essential dual-function complex mediates erythrocyte invasion and channel-mediated nutrient uptake in malaria parasites. *Elife,* 6**,** e23485.

JIMENEZ-DIAZ, M. B., EBERT, D., SALINAS, Y., PRADHAN, A., LEHANE, A. M., MYRAND-LAPIERRE, M. E., O'LOUGHLIN, K. G., SHACKLEFORD, D. M., JUSTINO DE ALMEIDA, M., CARRILLO, A. K., CLARK, J. A., DENNIS, A. S., DIEP, J., DENG, X., DUFFY, S., ENDSLEY, A. N., FEDEWA, G., GUIGUEMDE, W. A., GOMEZ, M. G., HOLBROOK, G., HORST, J., KIM, C. C., LIU, J., LEE, M. C., MATHENY, A., MARTINEZ, M. S., MILLER, G., RODRIGUEZ-ALEJANDRE, A., SANZ, L., SIGAL, M., SPILLMAN, N. J., STEIN, P. D., WANG, Z., ZHU, F., WATERSON, D., KNAPP, S., SHELAT, A., AVERY, V. M., FIDOCK, D. A., GAMO, F. J., CHARMAN, S. A., MIRSALIS, J. C., MA, H., FERRER, S., KIRK, K., ANGULO-BARTUREN, I., KYLE, D. E., DERISI, J. L., FLOYD, D. M. & GUY, R. K. 2014. (+)-SJ733, a clinical candidate for malaria that acts through ATP4 to induce rapid host-mediated clearance of Plasmodium. *Proc Natl Acad Sci U S A,* 111**,** E5455-62.

Molecular Pharmacology Fast Forward. Published on July 7, 2022 as DOI: 10.1124/molpharm.122.000549
This article has not been copyedited and formatted. The final version may differ from this version.

KROGSTAD, D. J., GLUZMAN, I. Y., KYLE, D. E., ODUOLA, A. M., MARTIN, S. K., MILHOUS, W. K. & SCHLESINGER, P. H. 1987. Efflux of chloroquine from Plasmodium falciparum: mechanism of chloroquine resistance. *Science,* 238**,** 1283-5.

KUTNER, S., BARUCH, D., GINSBURG, H. & CABANTCHIK, Z. I. 1982. Alterations in membrane permeability of malaria-infected human erythrocytes are related to the growth stage of the parasite. *Biochim Biophys Acta,* 687**,** 113-7.

LISK, G. & DESAI, S. A. 2005. The plasmodial surface anion channel is functionally conserved in divergent malaria parasites. *Eukaryot Cell,* 4**,** 2153-9.

LISK, G., PAIN, M., GLUZMAN, I. Y., KAMBHAMPATI, S., FURUYA, T., SU, X. Z., FAY, M. P., GOLDBERG, D. E. & DESAI, S. A. 2008. Changes in the plasmodial surface anion channel reduce leupeptin uptake and can confer drug resistance in Plasmodium falciparum-infected erythrocytes. *Antimicrob Agents Chemother,* 52**,** 2346-54.

LUTH, M. R., GUPTA, P., OTTILIE, S. & WINZELER, E. A. 2018. Using in Vitro Evolution and Whole Genome Analysis To Discover Next Generation Targets for Antimalarial Drug Discovery. *ACS Infect Dis,* 4**,** 301-314.

MARSHALL, N. J., GOODWIN, C. J. & HOLT, S. J. 1995. A critical assessment of the use of microculture tetrazolium assays to measure cell growth and function. *Growth Regul,* 5**,** 69-84.

MIRA-MARTINEZ, S., ROVIRA-GRAELLS, N., CROWLEY, V. M., ALTENHOFEN, L. M., LLINAS, M. & CORTES, A. 2013. Epigenetic switches in clag3 genes mediate blasticidin S resistance in malaria parasites. *Cell Microbiol,* 15**,** 1913-23.

NGUITRAGOOL, W., BOKHARI, A. A., PILLAI, A. D., RAYAVARA, K., SHARMA, P., TURPIN, B., ARAVIND, L. & DESAI, S. A. 2011. Malaria Parasite clag3 Genes Determine Channel-Mediated Nutrient Uptake by Infected Red Blood Cells. *Cell,* 145**,** 665-77.

NOEDL, H., SE, Y., SCHAECHER, K., SMITH, B. L., SOCHEAT, D. & FUKUDA, M. M. 2008. Evidence of artemisinin-resistant malaria in western Cambodia. *N Engl J Med,* 359**,** 2619-20.

OVERMAN, R. R. 1948. Reversible cellular permeability alterations in disease; in vivo studies on sodium, potassium and chloride concentrations in erythrocytes of the malarious monkey. *Am J Physiol,* 152**,** 113-21.

PATH 2011. *Staying the Course? Malaria Research and Development in a Time of Economic Uncertainty.,* Seattle, Program for Appropriate Technology in Health.

PHYO, A. P., NKHOMA, S., STEPNIEWSKA, K., ASHLEY, E. A., NAIR, S., MCGREADY, R., LER MOO, C., AL-SAAI, S., DONDORP, A. M., LWIN, K. M., SINGHASIVANON, P., DAY, N. P., WHITE, N. J., ANDERSON, T. J. & NOSTEN, F. 2012. Emergence of artemisinin-resistant malaria on the western border of Thailand: a longitudinal study. *Lancet,* 379**,** 1960-6.

PILLAI, A. D., ADDO, R., SHARMA, P., NGUITRAGOOL, W., SRINIVASAN, P. & DESAI, S. A. 2013. Malaria parasites tolerate a broad range of ionic environments and do not require host cation remodelling. *Mol Microbiol,* 88**,** 20-34.

PILLAI, A. D., NGUITRAGOOL, W., LYKO, B., DOLINTA, K., BUTLER, M. M., NGUYEN, S. T., PEET, N. P., BOWLIN, T. L. & DESAI, S. A. 2012. Solute Restriction Reveals an Essential Role for clag3-Associated Channels in Malaria Parasite Nutrient Acquisition. *Mol Pharmacol,* 82**,** 1104-1114.

PILLAI, A. D., PAIN, M., SOLOMON, T., BOKHARI, A. A. & DESAI, S. A. 2010. A cell-based high-throughput screen validates the plasmodial surface anion channel as an antimalarial target. *Mol Pharmacol,* 77**,** 724-33.

SCHURECK, M. A., DARLING, J. E., MERK, A., SHAO, J., DAGGUPATI, G., SRINIVASAN, P., OLINARES, P. D. B., ROUT, M. P., CHAIT, B. T., WOLLENBERG, K., SUBRAMANIAM,

S. & DESAI, S. A. 2021. Malaria parasites use a soluble RhopH complex for erythrocyte invasion and an integral form for nutrient uptake. *Elife,* 10.

SENGUPTA, D., GHARBAOUI, T., KRISHNAN, A., BUZARD, D. J., JONES, R. M., MA, Y. A., BURDA, R., MONTALBAN, A. G. & SEMPLE, G. 2015. An Efficient Scale-Up Process for the Preparation of the APD334 Precursor 4-Chloromethyl-1-cyclopentyl-2-(trifluoromethyl)benzene. *Organic Process Research & Development* 19**,** 618-623.

SHARMA, P., RAYAVARA, K., ITO, D., BASORE, K. & DESAI, S. A. 2015. A CLAG3 mutation in an amphipathic transmembrane domain alters malaria parasite nutrient channels and confers leupeptin resistance. *Infect Immun,* 83**,** 2566-74.

SHARMA, P., WOLLENBERG, K., SELLERS, M., ZAINABADI, K., GALINSKY, K., MOSS, E., NGUITRAGOOL, W., NEAFSEY, D. & DESAI, S. A. 2013. An epigenetic antimalarial resistance mechanism involving parasite genes linked to nutrient uptake. *J Biol Chem,* 288**,** 19429-40.

STAINES, H. M., ALKHALIL, A., ALLEN, R. J., DE JONGE, H. R., DERBYSHIRE, E., EGEE, S., GINSBURG, H., HILL, D. A., HUBER, S. M., KIRK, K., LANG, F., LISK, G., OTENG, E., PILLAI, A. D., RAYAVARA, K., ROUHANI, S., SALIBA, K. J., SHEN, C., SOLOMON, T., THOMAS, S. L., VERLOO, P. & DESAI, S. A. 2007. Electrophysiological studies of malaria parasite-infected erythrocytes: current status. *Int J Parasitol,* 37**,** 475-82.

STEWART, B. H., CHAN, O. H., LU, R. H., REYNER, E. L., SCHMID, H. L., HAMILTON, H. W., STEINBAUGH, B. A. & TAYLOR, M. D. 1995. Comparison of intestinal permeabilities determined in multiple in vitro and in situ models: relationship to absorption in humans. *Pharm Res,* 12**,** 693-9.

VEIGA, M. I., DHINGRA, S. K., HENRICH, P. P., STRAIMER, J., GNADIG, N., UHLEMANN, A. C., MARTIN, R. E., LEHANE, A. M. & FIDOCK, D. A. 2016. Globally prevalent PfMDR1 mutations modulate Plasmodium falciparum susceptibility to artemisinin-based combination therapies. *Nat Commun,* 7**,** 11553.

WAGNER, M. A., ANDEMARIAM, B. & DESAI, S. A. 2003. A two-compartment model of osmotic lysis in Plasmodium falciparum-infected erythrocytes. *Biophys J,* 84**,** 116-23.

WALSKY, R. L. & OBACH, R. S. 2004. Validated assays for human cytochrome P450 activities. *Drug Metab Dispos,* 32**,** 647-60.

WHO 2013. World Malaria Report 2013; https://www.who.int/publications/i/item/9789241564694.

WHO. 2020. World malaria report 2020; https://www.who.int/publications/i/item/9789240015791.

Molecular Pharmacology Fast Forward. Published on July 7, 2022 as DOI: 10.1124/molpharm.122.000549
This article has not been copyedited and formatted. The final version may differ from this version.

Footnotes

This work was supported by the National Institutes of Health National Institute of Allergy and Infectious Diseases [Grants R43 (Phase I) and R44 (Phases II and IIB) AI100339]; the Intramural Research Program of the National Institutes of Health National Institute of Allergy and Infectious Diseases; and the Medicines for Malaria Venture (MMV). No author has an actual or perceived conflict of interest with the contents of this article.

Molecular Pharmacology Fast Forward. Published on July 7, 2022 as DOI: 10.1124/molpharm.122.000549
This article has not been copyedited and formatted. The final version may differ from this version.

Figure Legends.

Figure 1. *In vitro* potencies and ADME properties of select analogs of parent compound MBX-2366. [a]Activity in the uptake assay (μM); [b]*P. falciparum* growth inhibition (μM); [c]cytotoxicity against HeLa cells (μM); [d]solubility in water (μM); [e]murine liver microsome stability (t½ in minutes of 1 μM compound in the presence of NADPH at 37°C; [f]Caco-2 permeability, P_{app} x 10^{-6} cm/sec; [g]stability in the presence of mouse serum, % of compound consumed in 60 minutes; [h]percent protein bound by mouse plasma by equilibrium dialysis; [i]cytochrome P450 3A4 inhibition at 5 μM; NP, not performed.

Figure 2. Optimized pyridazinones inhibit PSAC and *P. falciparum* growth. (A) Screening hit MBX-2366, zones used to guide synthetic strategy, and key findings. **(B)** Structures and properties of MBX-2366 and optimized derivative MBX-4055. **(C)** Mean ± S.D. residual PSAC-mediated permeabilities (*P*) at indicated concentrations of MBX-2366, MBX-3318, and MBX-4055 (black, turquoise, and red symbols, respectively; *n* = 3-5 independent dose response trials for each inhibitor). Lines indicated best fits to the Langmuir isotherm: $P = a/(1 + (x / K_{0.5}))$. (**D)** Normalized *in vitro* parasite growth with indicated inhibitor concentrations in PGIM and RPMI (red and black symbols, respectively). Symbols reflect mean ± S.D. of triplicate wells in a dose response experiment and are representative of 2-5 trials for each compound. Improved killing in PGIM indicates action on nutrient acquisition and establishes primary action on nutrient acquisition. **(E)** Correlation between PSAC block and *in vitro* growth inhibition for 79 pyridazinone derivatives. Black, turquoise, and red symbols represent MBX-2366, MBX-3318, and MBX-4055, respectively. Pearson correlation coefficient for $K_{0.5}$ and IC_{50} values, $r = 0.81$; $p < 10^{-4}$.

Figure 3. Murine pharmacokinetics for MBX-4055. (A) Mean ± S.D. MBX-4055 and MBX-2366 plasma concentrations in mice after single dose administration (n = 3 per timepoint). MBX-

Molecular Pharmacology Fast Forward. Published on July 7, 2022 as DOI: 10.1124/molpharm.122.000549
This article has not been copyedited and formatted. The final version may differ from this version.

4055 at 30 mg/kg PO (red circles) or 10 mg/kg IV (orange triangles); MBX-2366 at 30 mg/kg PO (black circles). **(B)** Calculated pharmacokinetic parameters.

Figure 4. MBX-4055 exhibits broad spectrum activity and is refractory to acquired resistance. (A) Continuous recording of sorbitol-induced osmotic lysis without (black trace) or with 3.2, 16, 80, 400, 2000 nM MBX-4055. PSAC-mediated permeability is inversely proportional to the time to hemolysis. **(B)** Mean ± S.D. PSAC block $K_{0.5}$ and parasite growth inhibition IC_{50} values for MBX-4055 against indicated *P. falciparum* lines [red (left) and black (right) bars, respectively; n = 3-4 dose response experiments each]. The inhibitor retains broad activity against these lines, which represent all malaria-endemic continents and the full range of antimalarial susceptibilities. **(C)** MBX-4055 growth inhibition dose responses for Dd2 and $Dd2_{4055}$ (black circles and red triangles), showing unchanged potency against *in vitro* parasite growth after 6 months of *in vitro* selection (P = 0.1, n = 3). **(D)** Mean ± S.D. sorbitol permeability (P_s) at indicated [MBX-4055] for the parental Dd2 and $Dd2_{4055}$ lines (black circles and red triangles), normalized to 1.0 without inhibitor. There was a statistically insignificant change in MBX-4055 potency against the target (P = 0.1, n = 3). **(E)** Unchanged sorbitol permeability in $Dd2_{4055}$ (P = 0.49, n = 3), excluding upregulation of target activity by selective pressure.

Figure 5. Direct MBX-4055 action on PSAC in cell-attached and whole-cell patch-clamp. (A) Single channel recordings from trophozoite-infected erythrocytes at a -100 mV membrane voltage (V_m) with indicated [MBX-4055] added symmetrically to bath and pipette solutions. Red dashes indicate closed channel level. Note the long-blocked events when MBX-4055 is present. The schematic on the left shows the cell-attached patch-clamp configuration; inhibitor added to the pipette solution has direct access to channels in the membrane patch. **(B)** Cell-attached recording from a 3-channel patch before and after bath addition of MBX-4055 (top and bottom traces, respectively; final bath concentration, 210 nM). V_m, -100 mV. Dashed red lines represent

Molecular Pharmacology Fast Forward. Published on July 7, 2022 as DOI: 10.1124/molpharm.122.000549
This article has not been copyedited and formatted. The final version may differ from this version.

zero current, observed when all three channels are closed. Schematic shows inhibitor must cross the membrane to access channels in the patch. **(C)** All-points histogram of currents from the recordings in panel B tallied from 18.7 s of recording before and after MBX-4055 addition (black and red traces, respectively). The current levels corresponding to all channels closed (c), and 1, 2, or 3 channels open (o1, o2, o3) are indicated. **(D)** MBX-4055 dose-response experiments, determined using the whole-cell patch clamp method. Ensemble currents in response to V_m between -100 and +100 mV, applied in 10 mV increments, are shown from a single cell before and after sequential addition of MBX-4055 to indicated concentrations. Red dashes indicate zero current levels. Schematic illustrates this configuration with inhibitor addition to bath. **(E)** Mean ± S.D. chord conductance (γ) calculated from currents between V_m of -100 and 0 mV, normalized to 100 without inhibitor; all measurements from 4 cells were pooled. Red line, best fit to Langmuir isotherm, $\gamma = a/(1 + (x/K_{0.5}))$.

Molecular Pharmacology Fast Forward. Published on July 7, 2022 as DOI: 10.1124/molpharm.122.000549
This article has not been copyedited and formatted. The final version may differ from this version.

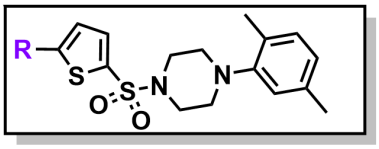

#	CMPD#	R	Target $K_{0.5}$[a]	IC_{50}[b]	CC_{50}[c]	Sol[d]	MLMS[e]	Caco-2 (Papp)[f]	MSS(% cons.)[g]	MPPB (% bound)[h]	Cyp 3A4 (% inhib.)[i]
1	ISG-21 MBX-2366	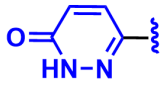	0.003	0.002	86	25	15.6	0.0	0	100	0
2	MBX-3248	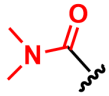	0.023	0.36	>200	50	6.0	65	35	99	16.5
3	MBX-3301	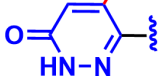	0.001	0.009	79	>200	4.7	0.0	5.2	>99.9	NP
4	MBX-5066	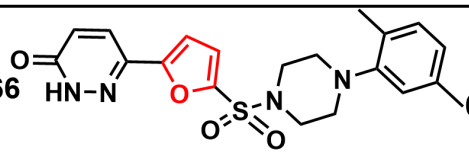	0.047	0.23	8.2	100	13.7	5.8	0	99	0

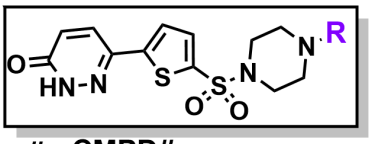

#	CMPD#	R	Target $K_{0.5}$[a]	IC_{50}[b]	CC_{50}[c]	Sol[d]	MLMS[e]	Caco-2 (Papp)[f]	MSS(% cons.)[g]	MPPB (% bound)[h]	Cyp 3A4 (% inhib.)[i]
5	MBX-3105	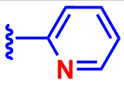	0.024	0.030	>200	25	5.6	0.0	1	99	11
6	MBX-2937	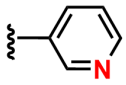	0.027	0.019	>200	25	14.5	6.5	3	99	67
7	MBX-3318		0.014	0.016	>200	25	7.7	11.2	0	96	0
8	MBX-3477A	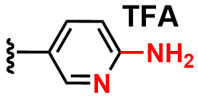	0.027	0.066	>200	>200	91.8	0.29	7	97	1
9	MBX-3976		0.017	0.007	>200	50	10.0	8.9	0	96	0
10	MBX-4055	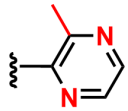	0.021	0.042	>200	50	26.5	7.8	5	94	0
11	MBX-6513	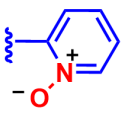	0.26	0.154	>200	50	>120	NP	NP	NP	NP

Figure 1

Molecular Pharmacology Fast Forward. Published on July 7, 2022 as DOI: 10.1124/molpharm.122.000549
This article has not been copyedited and formatted. The final version may differ from this version.

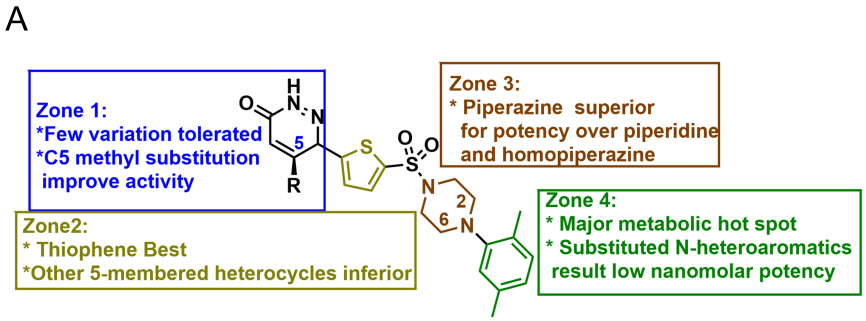

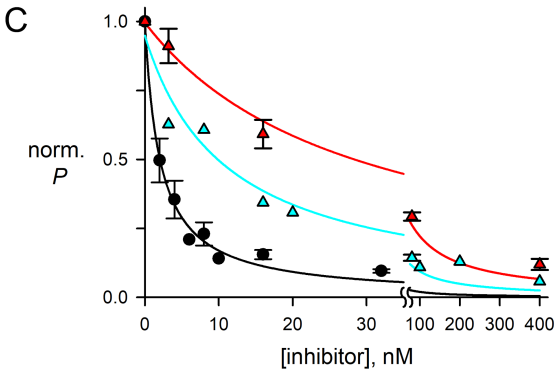

B

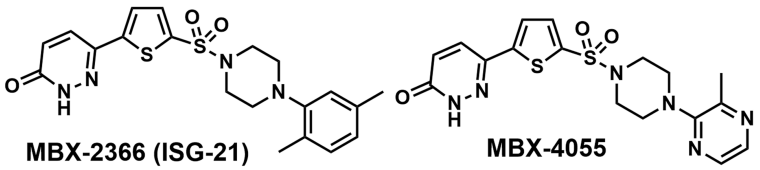

	MBX-2366	MBX-4055
PSAC inhibition $K_{0.5}$ =	3 nM	21 nM
P.falciparum growth inhibition IC_{50} =	2 nM	42 nM
CC_{50} (HeLa; 72 h) =	82	>200
Solubility limit in H_2O =	25 mM	25 mM
murine liver microsome stability ($t_{1/2}$) =	15.6 min	26.5 min
mouse serum stability (% consumed) =	0	5
mouse protein binding (% bound) =	100%	94%
CYP 3A4 (%inhibition) =	0	0
Caco-2; P_{app} (A - B) =	0.00	7.8 x10^{-6} cms^{-1}

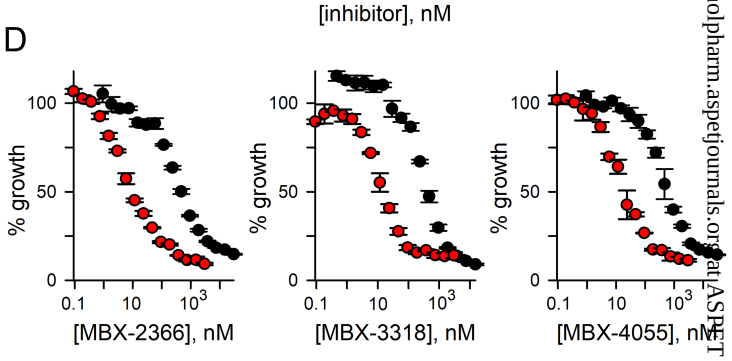

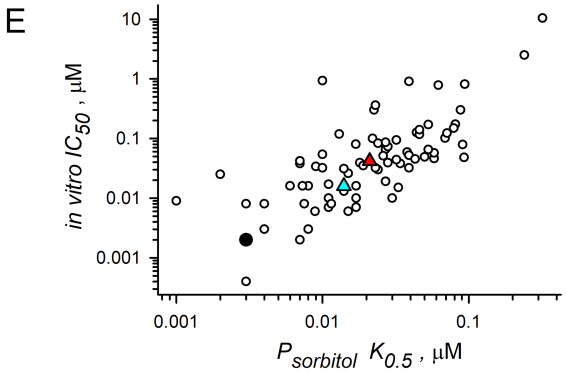

Figure 2

Molecular Pharmacology Fast Forward. Published on July 7, 2022 as DOI: 10.1124/molpharm.122.000549
This article has not been copyedited and formatted. The final version may differ from this version.

A

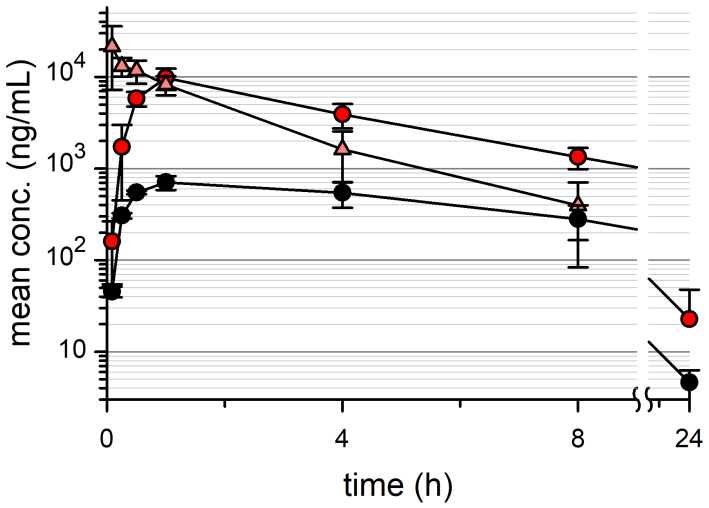

B

Compound, Dose	t½ (hr)	$C_{0/max}$ (ng/mL)	AUC_{last} (hr•ng/mL)	V_{ss} (mL/kg)	Cl (mL/hr/kg)	%F[a] (last)
MBX-4055, 10 mg/kg, IV	2.0	27,695	28,625	707	336	-
MBX-4055, 30 mg/kg, PO	2.58	9,797	46,904	-	-	55
MBX-2366, 30 mg/kg, PO	2.8	707	4,979	-	-	ND[b]

[a]Determined by dividing AUC_{last} for the PO dose (adjusted for the dose difference) by the AUC_{last} for the IV dose and multiplying by 100; [b]ND due to lack of IV data for comparison.

Figure 3

Molecular Pharmacology Fast Forward. Published on July 7, 2022 as DOI: 10.1124/molpharm.122.000549
This article has not been copyedited and formatted. The final version may differ from this version.

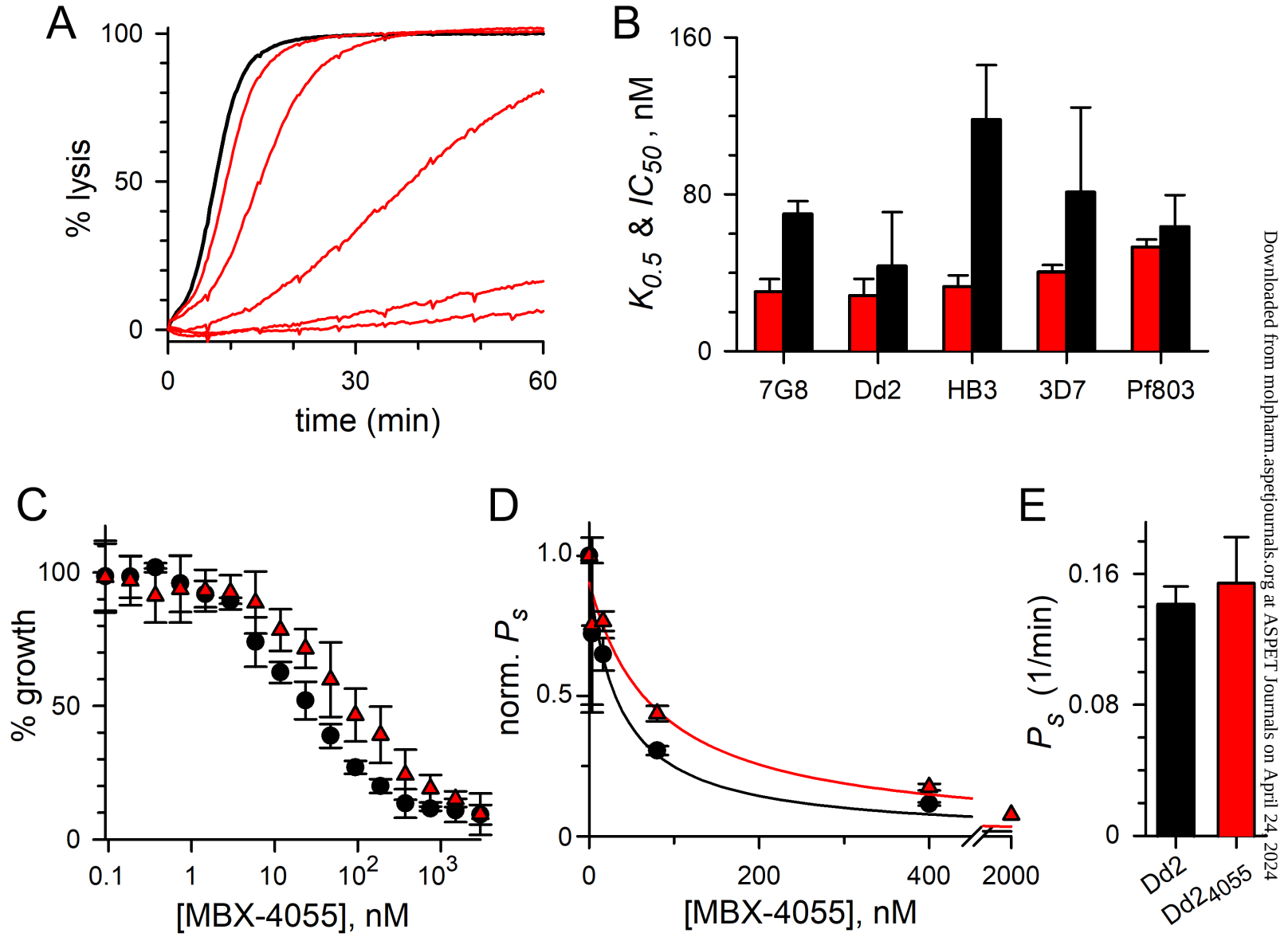

Figure 4

Molecular Pharmacology Fast Forward. Published on July 7, 2022 as DOI: 10.1124/molpharm.122.000549
This article has not been copyedited and formatted. The final version may differ from this version.

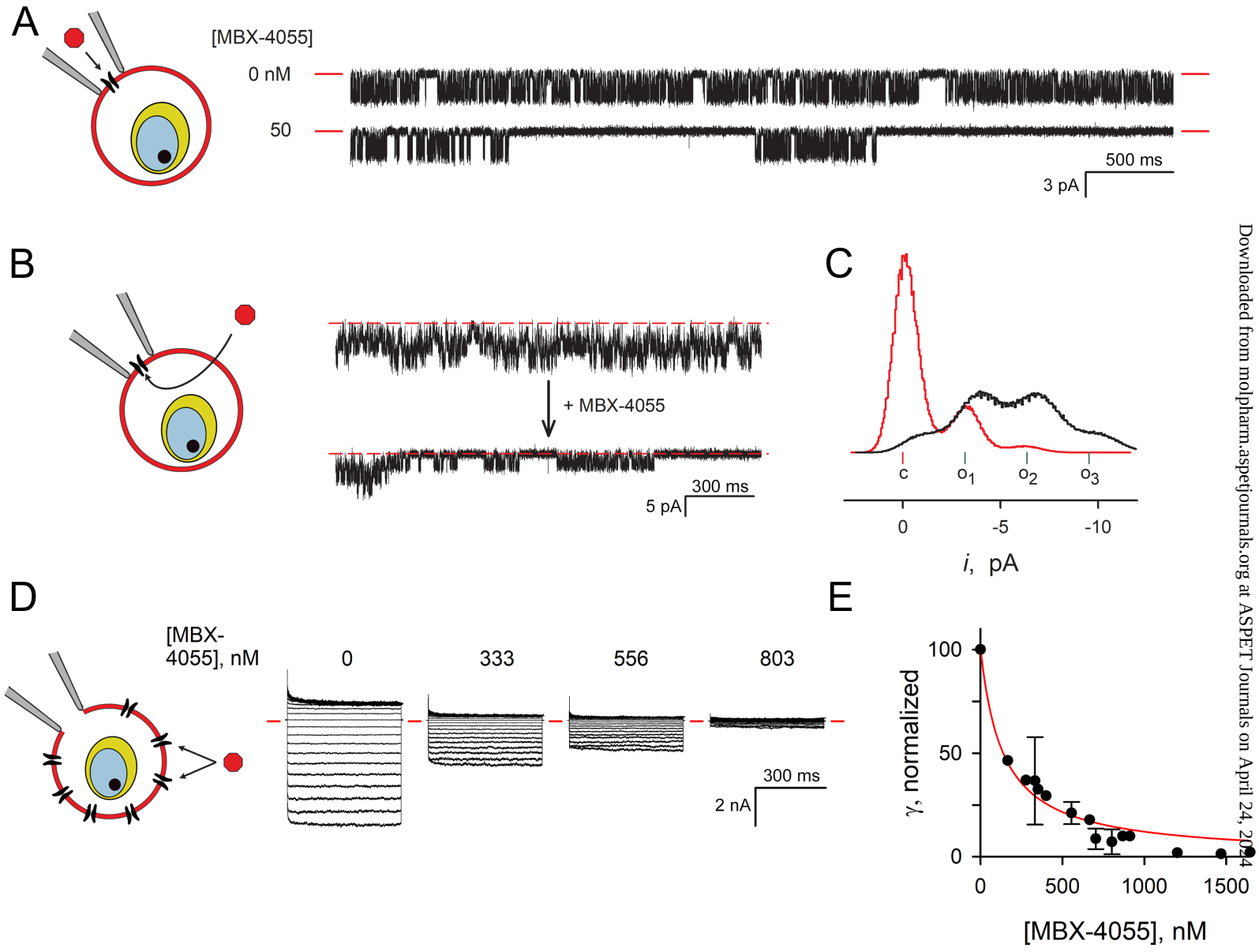

Figure 5